Journal of Quantitative Spectroscopy & Radiative Transfer 208 (2018) 179–187

Contents lists available at ScienceDirect

Journal of Quantitative Spectroscopy & Radiative Transfer

journal homepage: www.elsevier.com/locate/jqsrt

The absorption spectrum of acetylene near 1 μm (9280–10740 cm^{-1}) (I): Line positions

O.M. Lyulin[a,b], S. Béguier[a], S.M. Hu[c,d], A. Campargue[a,*]

[a] University of. Grenoble Alpes, CNRS, LIPhy, Grenoble 38000, France
[b] Laboratory of Theoretical Spectroscopy, V.E. Zuev Institute of Atmospheric Optics SB RAS, 1, Academician Zuev square, Tomsk 634021, Russia
[c] Hefei National Laboratory for Physical Sciences at Microscale, iChem Center, University of Science and Technology of China, Hefei 230026, China
[d] CAS Center for Excellence and Synergetic Innovation Center in Quantum Information and Quantum Physics, University of Science and Technology of China, Hefei 230026 China

ARTICLE INFO

Article history:
Received 8 December 2017
Revised 5 January 2018
Accepted 5 January 2018
Available online 6 January 2018

Keywords:
Acetylene
C_2H_2
Effective Hamiltonian
FTS
Spectroscopic database
HITRAN

ABSTRACT

The high-resolution absorption spectrum of acetylene is studied by Fourier-transform spectroscopy (FTS) in the 9280–10740 cm^{-1} region dominated by the $3\nu_3$ band near 9640 cm^{-1}. Line positions and intensities of 1899 $^{12}C_2H_2$ and 151 $^{12}C^{13}CH_2$ absorption lines are retrieved from a spectrum recorded at room temperature (298.5 K) with a pressure of 87.6 hPa and a path length of 105 m. The measured $^{12}C_2H_2$ lines belong to thirty-three bands, twelve of them being newly assigned. The lines of $^{12}C^{13}CH_2$ in normal abundance (2.2%) belong to seven bands. For comparison the HITRAN database in the same region includes 301 lines of four $^{12}C_2H_2$ bands. Spectroscopic parameters of the upper vibrational levels are derived from band-by-band fits of the line positions (typical *rms* values are on the order of 0.002 cm^{-1}). The comparison to the HITRAN line list and to results obtained using the global effective operator approach reveals a number of significant deviations. The occurrence of local rovibrational perturbations affecting a number of the analyzed bands is illustrated by the case of the strong $3\nu_3$ band.

1. Introduction

In spite of being the most studied four-atoms molecule and of increasing needs for planetary applications, the status of the spectroscopic databases of acetylene (C_2H_2) in the near infrared is not satisfactory in terms of completeness and accuracy. Two major reasons explain this matter of fact: the lack of intensity information and the increasing difficulty in assigning the spectrum at high energy. While a number of studies have been devoted to rovibrational assignment and line positions analysis, intensity information is generally missing. Due to the number and strength of rovibrational interactions, if we except the strong bands dominating the spectrum, the rovibrational assignment of many overlapping perturbed bands is not straightforward and a significant fraction of acetylene lines remains.

The present contribution takes part in a long standing project aiming at constructing an empirical database for acetylene in the near infrared. We have recently released a line list for the wide 5850–9415 cm^{-1} region (excluding the 6341–7000 cm^{-1} interval) [1] by gathering results of six studies by Fourier-transform spectroscopy (FTS) in the region of the strong bands [2–4] and Cavity Ring Down spectroscopy (CRDS) in the region of weak absorption windows between the bands [5–7]. Compared to the HITRAN [8] and GEISA [9] databases in the region, the number of bands (146) and lines (about 11000) was increased by one order of magnitude. In the present work, we follow a similar approach to extend our empirical database towards higher energy by revisiting the FTS spectrum in the 9280–10740 cm^{-1} interval.

In our preceding studies, the rovibrational analysis benefited from the predictions of the effective Hamiltonian (EH) model developed at IAO-Tomsk [10,11] which allowed identifying additional bands in previously recorded spectra. This model is a polyad model. Vibrational states in strong resonance interaction form polyads characterized by the polyad quantum number, $P = 5V_1 + 3V_2 + 5V_3 + V_4 + V_5$. [The $(V_1V_2V_3V_4V_5l_4l_5)$ conventional normal modes are used for the vibrational labelling where V_i are the vibrational normal modes quantum numbers, and $i = 1$–5 correspond to the symmetric CH and CC stretching modes, the antisymmetric CH stretch, and the *trans*- and *cis*-degenerate bending modes, respectively. The latter are characterized by the bending angular momentum quantum numbers, l_4 and l_5]. Using

* Corresponding author.
E-mail address: alain.campargue@ujf-grenoble.fr (A. Campargue).

https://doi.org/10.1016/j.jqsrt.2018.01.007
0022-4073/

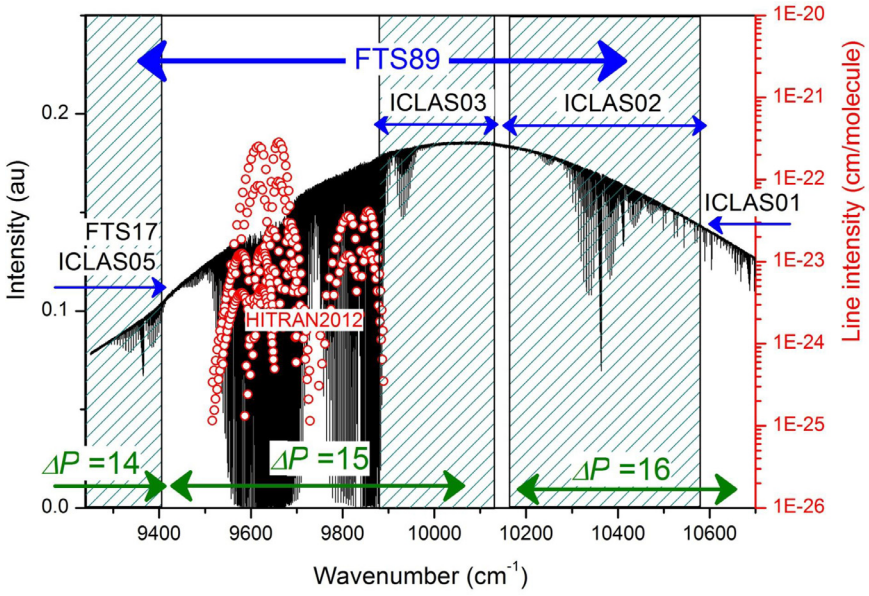

Fig. 1. Overview of the studied acetylene spectrum in the 9280–10740 cm^{-1} region recorded by Fourier transform spectroscopy (pressure of 87.6 hPa, path length of 105 m). The displayed region covers the entire ΔP = 15–16 series of bands and part of the ΔP = 14 series. The HITRAN2016 list is superimposed (right-hand logarithmic scale for line intensities). The range of previous studies is indicated: FTS89 [14], FTS17 [4], ICLAS01 [19], ICLAS02 [18], ICLAS03 [17] and ICLAS05 [15].

the EH eigenfunctions, the effective dipole moment (EDM) parameters of each ΔP series of bands were fitted to the available measured intensity values. As a result, the Tomsk model provides not only predicted line positions but also reasonable intensity values for most of the predicted bands. This is a key advantage in the assignment process.

An overview of the spectrum under analysis is presented in Fig. 1 together with the range of the most relevant previous analysis in the region. The HITRAN2016 line list included in Fig. 1 consists of the four strongest bands dominated by the $3\nu_3$ band at 9640 cm^{-1}. The HITRAN positions and intensities were obtained by FTS by Vander Auwera et al. [12] and Jacquemart et al. [13], respectively. The most exhaustive analysis in the region (9362–10413 cm^{-1}) was reported by Herman et al. in 1989 by FTS with 40 m path length and 9 Torr pressure [14]. Four intervals were studied by high sensitivity Intracavity Laser Absorption Spectroscopy (ICLAS). The spectra in the region below 9410 cm^{-1} and in the 9857–10118 cm^{-1} interval were recorded using a Vertical External Cavity Surface Emitting Laser (VECSEL). ICLAS-VECSEL provides typical detectivity at the $\alpha_{min} = 10^{-9}$ cm^{-1} level [15] *i. e.* significantly beyond the FTS sensitivity. Nevertheless, due to the VECSEL laser dynamics [16], ICLAS-VECSEL can hardly be used for quantitative spectroscopy and no line intensity information was provided. The spectra in the 10160–10570 cm^{-1} interval [18] and above 10600 cm^{-1} [19] were investigated by high sensitivity ICLAS using a Ti: Sapphire laser. Again no intensity information was retrieved in the region. Intensity measurements of the strongest bands in the 9000–9420 cm^{-1} region was very recently obtained by FTS [4] and incorporated in the empirical database [1].

In the present work, we use a high resolution FTS spectrum recorded at USTC–Hefei with a path length of 105 m to construct a line list and extend the assignments in the 9280–10740 cm^{-1} range. The spectrum assignments, comparison with databases and discussion of the rovibrational perturbation are presented in the next section of this paper. A companion paper will be devoted to line intensities and will include the derivation of the Herman–Wallis coefficients and of the ΔP = 15 and 16 EDM parameters, and the construction of a recommended line list in the region.

2. Experimental details, line list construction and rovibrational assignments

The FTS spectrum was recorded at USTC (Hefei, China) with a Bruker IFS 120 HR Fourier–transform spectrometer equipped with a multi-pass White cell adjusted to its maximum optical path length of 105 m. A tungsten source, a CaF_2 beam splitter and a Ge diode detector were used. The line positions were calibrated using the absorption lines of water (present as an impurity in the cell) given in HITRAN [8]. The unapodized resolution was 0.0142 cm^{-1}. The temperature and pressure were 298.5 K and 87.6 hPa, respectively.

A homemade multiline fitting computer code was used to derive the line positions and intensities. The line shape was modeled with the Voigt profile. The Doppler half width at half maximum was fixed to its theoretical value of about 0.011 cm^{-1}. The Lorentzian width of about 0.012 cm^{-1}, corresponding to an average pressure self broadening of 0.14 cm^{-1}/atm [2], was adjusted when necessary. The typical *rms* of the (Meas.–Sim.) residuals correspond to a noise equivalent absorption $\alpha_{min} \approx 3 \times 10^{-7}$ cm^{-1} which leads to smallest measured line intensities on the order of a few 10^{-26} cm/molecule. We estimate the accuracy of the intensities reported in the present work to be about 15% for relatively strong isolated lines. Overall, line centers and intensities were derived for a set of about 3000 lines. A number of lines due to water observed in the high energy part of the spectrum were manually removed from the line list, leaving about 2500 lines to be assigned.

3. Rovibrational assignments

As mentioned above, the $^{12}C_2H_2$ rovibrational assignments relied on previous studies and on the predictions of the effective Hamiltonian model developed in Tomsk in the frame of the effective operator approach [10]. This model considers all the resonance interactions between rovibrational levels up to the ninth order of perturbation theory. Effective rovibrational parameters were adjusted to reproduce about 25,000 measured line positions collected from the literature up to 9900 cm^{-1}. The usual criteria (presence of a *Q* branch, observation of the 1:3 intensity alternation from even

to odd values of J) and lower state combination difference (GSCD) relations were systematically used to establish the assignments. The intensity information provided by the model was a key criterion in the assignment process. The line intensity modeling uses the eigenfunctions of the refined effective Hamiltonian [10] and EDM parameters fitted against experimental intensity values. The $\Delta P = 15$ parameters were obtained in Ref. [20] from a fit of the FTS intensity values of the four bands measured by Jacquemart et al. [13] (mostly identical to the HITRAN dataset). The $\Delta P = 16$ EDM parameters were not yet determined and rough estimated values were used to help the assignments.

Overall, 1899 $^{12}C_2H_2$ lines were assigned to thirty-three bands, twelve of them being newly assigned. The bands are listed in Table 1 in increasing order of the upper state energy. In the first column, we provide the $(v_1 v_2 v_3 v_4 v_5 l_4 l_5 \varepsilon)$ normal mode labeling and symmetry type (e or f) relative to the Wang transformation. The vibrational labeling was obtained from the refined global effective Hamiltonian [10] and corresponds to the maximum fraction of the low J eigenfunctions in the normal mode basis. We also give the band name in the vibrational notation of Plíva adopted in the HITRAN database: $v_1\ v_2\ v_3 (v_4\ v_5)^{\ell\pm} r$ with $\ell = |\ell_4 + \ell_5|$, ℓ_t being the vibrational angular momentum quantum number associated with the degenerated bending mode t, $\pm$ being the symmetry type for Σ vibrational states ($\ell = 0$), and r a roman numeral indicating the rank of the level, by decreasing energy value ($r = I$ for the highest energy level), inside the set of states having the same vibrational assignment.

As expected, most of the new bands are located in the strong absorbing spectral region which is highly congested and was not previously investigated by ICLAS. The higher sensitivity of the ICLAS technique provided observations below the detectivity threshold of the present FTS recordings: two, four and one additional $^{12}C_2H_2$ bands were reported in Refs. [15,17,18], respectively. We could extend the assignments for all the bands reported by Herman et al. [14] (see the highest J values measured in each branch included in Table 1). The $\Delta_g - \Delta_u$ $3\nu_3 + (\nu_4 + \nu_5)^2$ - $(\nu_4 + \nu_5)^2$ band of $^{12}C_2H_2$ reported in this reference is in fact the $3\nu_3$ band of $^{12}C^{13}CH_2$ at 9609.1 cm^{-1}.

As indicated in Fig. 1, except for the previously studied $2\nu_1 + \nu_2 + \nu_5^1$ band at 9366.592 cm^{-1} belonging to the $\Delta P = 14$ series of bands [4], the other bands below and above 10100 cm^{-1}, belong to the $\Delta P = 15$ and 16 series, respectively. The $\Delta P = 15$ series involves cold bands, hot bands from the $V_4 = 1$ and $V_5 = 1$ bending levels and the $3\nu_3 + (\nu_4 + \nu_5)^0$-$(\nu_4 + \nu_5)^0$ Σ_g–Σ_u and $3\nu_3 + (\nu_4 + \nu_5)^2$-$(\nu_4 + \nu_5)^2$ Δ_g-Δ_u hot bands. The latter reach $P = 17$ levels around 10910 cm^{-1} which are the most excited levels identified in the analysis. The $\Delta P = 16$ bands are all cold bands, hot bands being too weak to be detected in this series. Note that the 0031010, 2011010 and 1020101 levels of the $P = 16$ polyad are observed as upper states of both a $\Delta P = 16$ Π_u–Σ_g^+ cold band and a $\Delta P = 15$ Π_u–Π_g hot band.

About 150 transitions of seven bands of $^{12}C^{13}CH_2$ in natural abundance (2.2 %) were identified. The identification relied on the extensive study by Di Lonardo et al. performed by FTS with 99 % enrichment in $H^{12}C^{13}CH$ and a 55.1 m path length [21] (the corresponding line positions can be found in Ref. [22]).

Fig. 2 shows an overview comparison of the list of assigned transitions to the HITRAN2016 list.

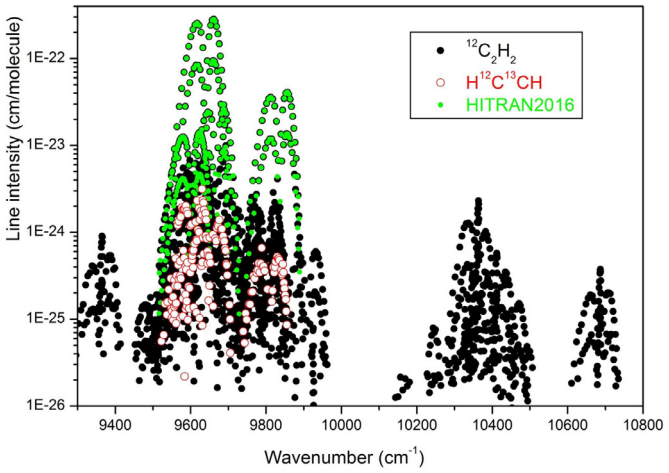

Fig. 2. Overview of the acetylene transitions assigned between 9280 and 10740 cm^{-1}. The $^{12}C_2H_2$ and $^{12}C^{13}CH_2$ lines are plotted with different symbols (black full circles and open red circles, respectively). The HITRAN2016 list of four bands of $^{12}C_2H_2$ is also displayed for comparison (green full circles). (For interpretation of the references to color in this figure legend, the reader is referred to the web version of this article.)

4. Band by band analysis

4.1. Spectroscopic parameters

The rotational analysis was performed using the standard formula for the rovibrational energy levels of an isolated vibrational state:

$$T(v, J, e/f) = G_{e/f} + B_{e/f} J(J+1) - D_{e/f}[J(J+1)]^2 + H_{e/f}[J(J+1)]^3 \quad (1)$$

where $G_{e/f}$ are the vibrational term values and $B_{e/f}$, $D_{e/f}$, and $H_{e/f}$ are the rotational and distorsion constants of the e and f sub levels. The parameters of the $^{12}C_2H_2$ and $^{12}C^{13}CH_2$ lower vibrational levels were constrained to their fitted values of Refs. [5,6] and Ref. [23], respectively. As the e and f sub bands may be perturbed in a different way, different sets of spectroscopic parameters were fitted for the e and f levels. The parameters of the 0031010, 2011010 and 1020101 upper levels were derived from a simultaneous fit of the line positions of the cold and hot bands reaching these three levels. The retrieved constants of the lower and upper states are listed in Table 1. The list of measured wavenumbers and intensities together with assignments and (obs.-calc) position values is provided as Supplementary Material. Part of the absorption lines of the four strong bands included in the HITRAN database were saturated in our spectrum. As indicated in the Supplementary Material, the accurate centers reported by Vander Auwera et al. [12] were used for saturated lines and gathered with our high J line centers to derive the band parameters of the four corresponding upper levels. About half of the studied bands were found to be affected by perturbations (they are marked with "p" in Table 1). After exclusion of the lines with poorly determined centers or affected by perturbation, the average *rms* values of the (meas.-fit) differences are on the order of 2×10^{-3} cm^{-1} which is the order of magnitude of the accuracy on the line measured positions. Overall, the *rms* values of the fit reported by ICLAS [15,17–19] are larger, in agreement with the claimed accuracy on the ICLAS line positions (0.005–0.01 cm^{-1}). Let us note that a few distortion constants are anomalously large or negative. This is most probably due to resonances which are reproduced in an effective way using the isolated band model of Eq. (1).

Table 1 includes a comparison of the spectroscopic parameters to literature values. The comparison considers not only bands previously observed in the region but also bands located in a different range reaching one of the observed upper levels. Among the upper levels of the twelve newly reported bands, three were previously detected in other spectral regions. Overall the agreement with literature values is satisfactory. Nevertheless, we note a systematic

Table 1
Spectroscopic parameters (in cm^{-1}) of the rovibrational bands of $^{12}C_2H_2$ and $^{12}C^{13}CH_2$ assigned in the FTS spectra of acetylene between 9280 and 10740 cm^{-1}. The bands are listed according to the increasing values of the upper state energy levels.

$^{12}C_2H_2$

Lower state constants [5,6]

$v_1v_2v_3v_4v_5l_4l_5\varepsilon$ [a]	$G_{e/f}$	$B_{e/f}$	$D_{e/f}\times10^6$	$H_{e/f}\times10^{10}$
0000000	0.0	1.1766462	1.6270	0.016
0001010e	611.693759	1.17532307	1.6405	0.0177
0001010f	611.693755	1.18055377	1.67973	0.0187
0000101e	729.15410	1.1764413	1.6326	0.017
0000101f	729.15410	1.1811398	1.6714	0.018
000111–1e	1328.0722	1.180508	3.595	2.76
000111–1f	1340.5507	1.1800836	1.715	
0001111f	1342.8023	1.179838	1.647	
0001111e	1342.8034	1.179804	-0.226	-2.78

Upper state constants

	$v_1v_2v_3v_4v_5l_4l_5\varepsilon$ [a]	*Fraction (%)* [b]	$G_{e/f}$	$B_{e/f}$	$D_{e/f}\times10^6$	$H_{e/f}\times10^{10}$	n_{fit}/N_{tot} [c]	Bands [d]	*Band type*	$\Delta G_{e/f}$ [e]	*observed lines* [f]	*rms* [g]		Previous reports [h]
	***P* = 14**													
	2100101e	86	9366.5922(7)	1.156908(6)	1.63(1)		35/46	$2\nu_1+\nu_2+\nu_5^1$	Π_u–Σ_g^+	9366.5922(7)	P27/R25	1.0		
			62/65	$2\nu_1+\nu_2+\nu_5^1$	Π_u–Σ_g^+	*9366.5922(6)*	*P33/R30*	*2.5*		*Camp05, Bég17*				
	2100101f	86	9366.5933(8)	1.161976(7)	1.72(1)		24/25	$2\nu_1+\nu_2+\nu_5^1$	Π_u–Σ_g^+	9366.5933(8)	Q27	0.8		
			33/34	$2\nu_1+\nu_2+\nu_5^1$	Π_u–Σ_g^+	*9366.5935(7)*	Q37	*2.1*		*Camp05, Bég17*				
			13	$2\nu_1+\nu_2+\nu_5^1$	Π_u–Σ_g^+	*9366.59*	*/Q17/R11*	*9.6*		*Herm89*				
	***P* = 15**													
	0030000e	59	9639.8675(5)	1.158374(4)	1.768(5)	0.23(2)	69/87	$3\nu_3$	Σ_u^+–Σ_g^+	9639.8675(5)	P45/R43	2.0	p	
			9639.8536(5)	*1.158356(3)*	*1.724(3)*		*61*	$3\nu_3$	Σ_u^+–Σ_g^+	*9639.8536(5)*	*P35/R35*	*2.5*		*Herm89*
			9639.8670(1)	*1.158386(2)*	*1.812(5)*	*0.59(3)*	*31/62*	$3\nu_3$	Σ_u^+–Σ_g^+	*9639.8670(1)*	*P31/R31*	*0.4*		*JVA02*
N	1112020e	85	9664.341(4)	1.16086(5)	9.5(2)	50(3)	22/49	$\nu_1+\nu_2+\nu_3+2\nu_4^2$	Δ_u–Σ_g^+	9664.341(4)	P39/R41	1.7	p	
			9664.335(3)	*1.16077(5)*	*7.9(2)*		*14/15*	$\nu_1+\nu_2+\nu_3+2\nu_4^2$-$\nu_4^1$	Δ_u–Π_g	*9052.641(3)*	*P15/Q14/R13*	*4.1*		*Bég17*
	1112000e	68	9668.1608(8)	1.16126(1)	-5.66(6)	-41.9(6)	45/74	$\nu_1+\nu_2+\nu_3+2\nu_4^0$	Σ_u^+–Σ_g^+	9668.1608(8)	P41/R35	3.5	p	
			9668.126(6)	*1.16203(5)*	*-2.02(8)*		*51*	$\nu_1+\nu_2+\nu_3+2\nu_4^0$	Σ_u^+–Σ_g^+	*9668.126(6)*	*P26/R25*	*21.7*		*Herm89*
			9668.1661(3)	*1.161029(9)*	*-7.57(7)*	*-92(2)*	*28/38*	$\nu_1+\nu_2+\nu_3+2\nu_4^0$	Σ_u^+–Σ_g^+	*9668.1661(3)*	*P23/R23*	*0.6*		*JVA02*
	030331–1e	46	9741.6340(9)	1.16633(2)	4.6(1)	-6(1)	35/48	$3\nu_2+(3\nu_4+3\nu_5)^{0+}$I	Σ_u^+–Σ_g^+	9741.6340(9)	P29/R27	1.7	p	
			9741.619(2)	*1.16642(2)*	*5.02(4)*		*43*	$2\nu_2+\nu_3+(2\nu_4+2\nu_5)^{0+}I$	Σ_u^+–Σ_g^+	*9741.619(2)*	*P15/R17*	*6.8*		*Herm89*
	012111–1e	46	9744.5579(8)	1.16437(2)	0.9(1)	10(1)	37/42	$\nu_2+2\nu_3+(\nu_4+\nu_5)^{0+}$	Σ_u^+–Σ_g^+	9744.5579(8)	P23/R23	2.1		
			9744.5467(8)	*1.16433(1)*	*0.58(5)*		*27*	$\nu_2+2\nu_3+(\nu_4+\nu_5)^{0+}$	Σ_u^+–Σ_g^+	*9744.5467(8)*	*P23/R23*	*2.2*		*Herm89*
N	021222–2e	48	9787.494(1)	1.16505(3)	9.9(2)	44(2)	34/36	$2\nu_2+\nu_3+(2\nu_4+2\nu_5)^{0+}$	Σ_u^+–Σ_g^+	9787.494(1)	P21/R19	1.9		
	2010000e	67	9835.1756(6)	1.157568(5)	1.614(8)	0.22(4)	74/76	$2\nu_1+\nu_3$	Σ_u^+–Σ_g^+	9835.1756(6)	P37/R39	1.1		
			9835.1633(4)	*1.157558(2)*	*1.586(2)*		*61*	$2\nu_1+\nu_3$	Σ_u^+–Σ_g^+	*9835.1633(4)*	*P29/R33*	*1.5*		*Herm89*
			9835.1760(1)	*1.157560(1)*	*1.586(3)*		*40/43*	$2\nu_1+\nu_3$	Σ_u^+–Σ_g^+	*9835.1760(1)*	*P23/R21*	*0.4*		*JVA02*
	1110200e	58	9909.9092(8)	1.16252(2)	4.58(7)	4.4(7)	35/49	$\nu_1+\nu_2+\nu_3+2\nu_5^0$	Σ_u^+–Σ_g^+	9909.9092(8)	P27/R27	1.5		
			9909.924(2)	1.16234(2)	4.03(2)		44/53		Σ_u^+–Σ_g^+	9909.924(2)	P20/R35	*6.9*		*Camp03*
			9909.887(6)	*1.16272(8)*	*5.3(2)*		*24*	$2\nu_1+\nu_2+(\nu_4+\nu_5)^2$	Δ_u–Σ_g^+	*9909.887(6)*	*P16/R18*	*12.0*		*Herm89*
	1300101e	88	9927.189(6)	1.15115(8)	1.3(2)		5/6	$\nu_1+3\nu_2+\nu_5^1$	Π_u–Σ_g^+	9927.189(6)	P17/R15	1.1		
	1300101f	88	9927.196(2)	1.156378(3)	1.48(9)		8/14	$\nu_1+3\nu_2+\nu_5^1$	Π_u–Σ_g^+	9927.194(2)	Q17	3.0		
							56/65	$\nu_1+3\nu_2+\nu_5^1$	Π_u–Σ_g^+	*9927.194(2)*	*P21/Q27/R21*	*6.3*		*Camp03*
	***P* = 16**													
	0031010e	55	10214.3740(6)	1.156907(6)	1.68(1)	0.23(9)	19/28	$3\nu_3+\nu_4^1$	Π_u–Σ_g^+	10214.3740(6)	P25/R27	2.1	p	
							54/72	$3\nu_3+\nu_4^1-\nu_4^1$	Π_u–Π_g	9602.6802(6)	P35/Q13/R31	2.8		
	0031010f	55	10214.3763(6)	1.162983(6)	178(1)	0.43(6)	64/74	$3\nu_3+\nu_4^1-\nu_4^1$	Π_u–Π_g	9602.6826(6)	P38/Q17/R35	1.8		
							81	$3\nu_3+\nu_4^1-\nu_4^1$	Π_u–Π_g	*9602.668*	*P24/ /R20*	*8.8*		*Herm89*

(*continued on next page*)

Table 1 (*continued*)

	Upper state constants													
	$v_1v_2v_3v_4v_5l_4l_5\varepsilon$ [a]	*Fraction (%)*[b]	$G_{e/f}$	$B_{e/f}$	$D_{e/f}\times10^6$	$H_{e/f}\times10^{10}$	n_{fit}/N_{tot}[c]	Bands[d]	*Band type*	$\Delta G_{e/f}$[e]	*observed lines* [f]	*rms*[g]		Previous reports[h]
	0031010ef						*63/67*	$3\nu_3+\nu_4^1$	Π_u–Σ_g^+	*10214.383(2)*	*P25/Q20/R28*	*6.0*		*Ding02*
							64/68	$3\nu_3+\nu_4^1-\nu_4^1$	Π_u–Π_g		*P20/R20*	*2.3*		*JVA02*
N	1021010f	45	10232.598(1)	1.16568(2)	6.9(1)		22/29	$\nu_1+2\nu_3+\nu_4^1-\nu_5^1$	Π_g–Π_u	9503.444(1)	P19/R15	2.0	p	
N	1021010e	45	10232.632(2)	1.15569(3)	-0.98(7)		13/28	$\nu_1+2\nu_3+\nu_4^1-\nu_5^1$	Π_g–Π_u	9503.477(2)	P18/R18	1.7	p	
N	1205010f	37	10245.707(1)	1.16750(3)	-3.3(1)		15/24	$\nu_1+2\nu_2+5\nu_4^1-\nu_5^1$	Π_g–Π_u	9516.553(1)	P15/R15	2.7		
N	1205010e	37	10245.745(3)	1.15596(4)	-4.3(1)		7/15	$\nu_1+2\nu_2+5\nu_4^1-\nu_5^1$	Π_g–Π_u	9516.591(3)	P17/R16	4.3		
N	1113010f	53	10255.377(1)	1.169216(5)			14/33	$\nu_1+\nu_2+\nu_3+3\nu_4^1-\nu_4^1$	Π_u–Π_g	9643.683(1)	P23/R20	2.4	p	
							14/16	$\nu_1+\nu_2+\nu_3+3\nu_4^1$	Π_u–Σ_g^+	*10255.386(2)*	*Q17*	*3.4*		*Ding02*
N	1113010e	53	10255.383(1)	1.15745(2)	-3.79(5)		16/30	$\nu_1+\nu_2+\nu_3+3\nu_4^1-\nu_4^1$	Π_u–Π_g	9643.689(1)	P21/R21	2.6	p	
N	012212–1f	37	10326.004(2)	1.17091(6)	15.6(5)	289(13)	12/19	$\nu_2+2\nu_3+(2\nu_4+\nu_5)\ ^1\Pi-\nu_4^1$	Π_u–Π_g	9714.310(2)	P17/R17	2.3		
N	012212–1e	37	10326.026(1)	1.16025(3)	3.0(1)		13/21	$\nu_2+2\nu_3+(2\nu_4+\nu_5)\ ^1\Pi-\nu_4^1$	Π_u–Π_g	9714.332(1)	P17/R17	3.7		
	120412–1e	25	10327.412(2)	1.16529(1)			9/14	$\nu_1+2\nu_2+(4\nu_4+\nu_5)^1\Pi$	Π_u–Σ_g^+	10327.412(2)	P17/R13	1.7		
	120412–1f	25	10327.416(3)	1.16675(9)	-3.5(6)		4/7	$\nu_1+2\nu_2+(4\nu_4+\nu_5)^1\Pi$	Π_u–Σ_g^+	10327.416(3)	Q11	1.3		
							33/36	$\nu_1+2\nu_2+(4\nu_4+\nu_5)^1\Pi$	Π_u–Σ_g^+	*10327.437(3)*	*P15/Q12/R14*	*7.6*		*Ding02*
	03043–23f	41	10336.696(2)	1.16857(2)			4/4	$3\nu_2+(4\nu_4+3\nu_5)\ ^1\Pi\Pi$	Π_u–Σ_g^+	10336.696(2)	Q13	2.5		
							24/34	$3\nu_2+(4\nu_4+3\nu_5)\ ^1\Pi\Pi$	Π_u–Σ_g^+	*10336.696(6)*	*P21/Q17/R17*	*10.1*		*Ding02*
	0030101f	37	10342.4974(9)	1.16543(1)	3.32(3)	4.0(3)	42/49	$3\nu_3+\nu_5^1-\nu_5^1$	Π_g–Π_u	9613.3433(9)	P34/R25	2.0	p	
	0030101e	37	10342.4981(8)	1.158035(5)	1.948(6)		33/47	$3\nu_3+\nu_5^1-\nu_5^1$	Π_g–Π_u	9613.3440(8)	P30/R30	2.0	p	
							66	$3\nu_3+\nu_5^1-\nu_5^1$	Π_g–Π_u	*9613.326*	*P26/Q5/R20*	*8.6*		*Herm89*
	1204101e	38	10349.4700(9)	1.16634(1)	6.00(3)		22/38	$\nu_1+2\nu_2+(4\nu_4+\nu_5)^1\Pi$	Π_u–Σ_g^+	10349.4700(9)	P25/R21	2.4	p	
							38/41	$\nu_1+2\nu_2+(4\nu_4+\nu_5)^1\Pi$	Π_u–Σ_g^+	*10349.481(2)*	*P22/R20*	*5.9*		*Ding02*
	1204101f	38	10349.464(2)	1.16128(4)	5.6(2)	37(3)	15/27	$\nu_1+2\nu_2+(4\nu_4+\nu_5)^1\Pi$	Π_u–Σ_g^+	10349.464(2)	Q28	1.9		
							21/21	$\nu_1+2\nu_2+(4\nu_4+\nu_5)^1\Pi$	Π_u–Σ_g^+	*10349.473(4)*	*Q22*	*8.1*		*Ding02*
	111212–1f	39	10351.5215(8)	1.166237(4)	2.332(4)		26/40	$\nu_1+\nu_2+\nu_3+(2\nu_4+\nu_5)\ ^1\Pi-\nu_5^1$	Π_g–Π_u	9622.3674(8)	P36/R23	3.6	p	
	111212–1e	39	10351.5321(8)	1.159238(7)	2.61(1)		29/47	$\nu_1+\nu_2+\nu_3+(2\nu_4+\nu_5)\ ^1\Pi-\nu_5^1$	Π_g–Π_u	9622.3780(8)	P33/R26	2.1	p	
							22	$\nu_1+2\nu_2+(3\nu_4+2\nu_5)\ ^1\Pi-\nu_5^1$	Π_g–Π_u	9622.367	*P9/ /R7*	10.8		*Herm89*
	1020101f	71	10364.8270(7)	1.162271(5)	1.490(7)		19/31	$\nu_1+2\nu_3+\nu_5^1$	Π_u–Σ_g^+	10364.825(1)	Q31	1.3	p	
N							21/23	$\nu_1+2\nu_3+\nu_5^1-\nu_4^1$	Π_u–Π_g	9753.1332(7)	P18/R24	4.0		
							30/32	$\nu_1+2\nu_3+\nu_5^1$	Π_u–Σ_g^+	*10364.844(2)*	*Q32*	*5.6*		*Ding02*
	1020101e	71	10364.8286(7)	1.158146(6)	0.570(9)		36/54	$\nu_1+2\nu_3+\nu_5^1$	Π_u–Σ_g^+	10364.8280(7)	P31/R26	2.4	p	
N							17/21	$\nu_1+2\nu_3+\nu_5^1-\nu_4^1$	Π_u–Π_g	9753.1348(7)	P19/R15	4.3		
							47/59	$\nu_1+2\nu_3+\nu_5^1$	Π_u–Σ_g^+	*10364.831(2)*	*P33/R26*	*7.3*		*Ding02*
							34	$\nu_1+2\nu_3+\nu_5^1$	Π_u–Σ_g^+	*10364.809*	*P19/Q23/R15*	*9.7*		*Herm89*
N	1112101f	37	10375.572(4)	1.16132(3)	1.09(4)		9/12	$\nu_1+\nu_2+\nu_3+(2\nu_4+\nu_5)\ ^1\Pi-\nu_5^1$	Π_g–Π_u	9646.418(4)	P23/R21	1.5		
N	1112101e	37	10375.616(3)	1.16414(6)	-2.2(3)	-40(4)	12/14	$\nu_1+\nu_2+\nu_3+(2\nu_4+\nu_5)\ ^1\Pi-\nu_5^1$	Π_g–Π_u	9646.462(3)	P22/R20	4.2		
	2011010f	63	10413.5378 (7)	1.16187(1)	1.72(4)		23/26	$2\nu_1+\nu_3+\nu_4^1$	Π_u–Σ_g^+	10413.5378 (7)	Q26	1.7		
							41/49	$2\nu_1+\nu_3+\nu_4^1-\nu_4^1$	Π_u–Π_g	9801.8440(7)	P28/R26	1.3		
	2011010e	63	10413.5380(5)	1.156439(4)	1.607(5)		35/51	$2\nu_1+\nu_3+\nu_4^1$	Π_u–Σ_g^+	10413.5380(5)	P29/R27	1.5	p	
							34/55	$2\nu_1+\nu_3+\nu_4^1-\nu_4^1$	Π_u–Π_g	9801.8442(5)	P30/R28	1.5		
							72/79	$2\nu_1+\nu_3+\nu_4^1$	Π_u–Σ_g^+	*10413.542(1)*	*P21/Q26/R33*	*5.3*		*Ding02*
								$2\nu_1+\nu_3+\nu_4^1$	Π_u–Σ_g^+		*Q16*	*7.2*		*Herm89*
							81	$2\nu_1+\nu_3+\nu_4^1-\nu_4^1$	Π_u–Π_g	*10413.52*	*P26/Q2//R24*			*Herm89*
	1210000e	79	10450.3911(7)	1.152556(7)	1.91(1)		35/44	$\nu_1+2\nu_2+\nu_3$	Σ_u^+–Σ_g^+	10450.3911(7)	P27/R25	1.6		
			10450.392(1)	*1.152530(5)*	*1.832(5)*		*55/56*	$\nu_1+2\nu_2+\nu_3$	Σ_u^+–Σ_g^+	*10450.392(1)*	*P25/R33*	*4.0*		*Ding02*
	130111–1e	47	10475.036(1)	1.15577(1)	4.49(3)		15/22	$\nu_1+3\nu_2+(\nu_4+\nu_5)^{0+}$	Σ_u^+–Σ_g^+	10475.036(1)	P23/R15	2.3		
			10475.034(2)	*1.15582(3)*	*4.56(5)*		*40/45*	$\nu_1+3\nu_2+(\nu_4+\nu_5)^{0+}$	Σ_u^+–Σ_g^+	*10475.034(2)*	*P23/R25*	*7.8*		*Ding02*
N	2010101f	59	10530.9052(8)	1.162206(5)	1.631(7)		31/47	$2\nu_1+\nu_3+\nu_5^1-\nu_5^1$	Π_g–Π_u	9801.7511(8)	P27/R29	1.2	p	
N	2010101e	59	10530.9066(7)	1.157224(4)	1.571(5)		41/51	$2\nu_1+\nu_3+\nu_5^1-\nu_5^1$	Π_g–Π_u	9801.7525(7)	P28/R30	1.3		
N	3001010e	83	10566.325(1)	1.15526(1)	1.62(2)		15/23	$3\nu_1+\nu_4^1-\nu_5^1$	Π_g–Π_u	9837.171(1)	P20/Q1/R22	1.9		
N	3001010f	83	10566.340(2)	1.16044(2)	1.58(2)		6/9	$3\nu_1+\nu_4^1-\nu_5^1$	Π_g–Π_u	9837.186(2)	P19/R23	1.6		

(*continued on next page*)

Table 1 (*continued*)

	Upper state constants												
	$v_1v_2v_3v_4v_5l_4l_5\varepsilon$ [a]	*Fraction (%)*[b]	$G_{e/f}$	$B_{e/f}$	$D_{e/f}\times10^6$	$H_{e/f}\times10^{10}$	n_{fit}/N_{tot}[c]	Bands[d]	*Band type*	$\Delta G_{e/f}$[e]	*observed lines* [f]	*rms*[g]	Previous reports[h]
	3000101e	90	10688.4635(8)	1.155958(8)	1.62(2)		33/47	$3\nu_1+\nu_5{}^1$	Π_u–$\Sigma_g{}^+$	10688.4635(8)	P27/R25	1.1	
	3000101f	90	10688.4654(9)	1.160838(7)	1.64(1)		22/26	$3\nu_1+\nu_5{}^1$	Π_u–$\Sigma_g{}^+$	10688.4654(9)	Q27	0.7	
							64/67	$3\nu_1+\nu_5{}^1-\nu_4{}^1$	Π_u–Π_g	*10076.791(2)*	*P23/R21*	*6.7*	*Camp03*
							94/106	$3\nu_1+\nu_5{}^1$	Π_u–$\Sigma_g{}^+$	*10688.4654(7)*	*P36/Q37/R36*	*4.2*	*Weir01*
	$P=17$												
N	003111–1e	39	10908.539(1)	1.16268(1)	4.43(2)		21/28	$3\nu_3+(\nu_4+\nu_5)^{0+}-(\nu_4+\nu_5)^{0+}$	$\Sigma_g{}^+$–$\Sigma_u{}^+$	9580.467(1)	P27/R16	5.0	
N	003111–1f	39	10918.2826(9)	1.162122(8)	1.81(2)		31/37	$3\nu_3+(\nu_4+\nu_5)^{0-}-(\nu_4+\nu_5)^{0-}$	$\Sigma_g{}^-$–$\Sigma_u{}^-$	9577.7319(9)	P27/R21	3.8	
N	0031111e	37	10919.770(2)	1.16281(3)	-0.8(1)	-4(1)	12/14	$3\nu_3+(\nu_4+\nu_5)^2-(\nu_4+\nu_5)^2$	Δ_g–Δ_u	9576.968(2)	P28/R14	3.9	
N	0031111f	37	10919.773(2)	1.16272(2)	1.80(2)		9/12	$3\nu_3+(\nu_4+\nu_5)^2-(\nu_4+\nu_5)^2$	Δ_g–Δ_u	9576.971(2)	P25/R15	2.7	

$^{13}C^{12}CH_2$

$v_1v_2v_3v_4v_5l_4l_5\varepsilon$[a]	$G_{e/f}$	$B_{e/f}$	$D_{e/f}\times10^6$
0000000 [23]	0.0	1.1484335	1.5256

	Upper state constants $v_1v_2v_3v_4v_5l_4l_5\varepsilon$[a]	$G_{e/f}$	$B_{e/f}$	$D_{e/f}\times10^6$	$H_{e/f}\times10^{10}$	n_{fit}/N_{tot}[c]	Bands[d]	*Band type*	$\Delta G_{e/f}$[e]	*observed lines*[f]	*rms*[g]	Previous reports [h]
	***P*=15**												
	030331–1e	9593.346(2)	1.13811(2)	5.33(5)		15/15	$3\nu_2+(3\nu_4+3\nu_5)^{0+}$	$\Sigma_u{}^+$–$\Sigma_g{}^+$	9593.346(2)	P22/R17	4.9	
		9593.3518(6)	*1.13783(1)*	*3.40(6)*	*-30.4(6)*	*38*	$3\nu_2+(3\nu_4+3\nu_5)^{0+}$	$\Sigma_u{}^+$–$\Sigma_g{}^+$	*9593.3518(6)*	*P25/R23*	*1.8*	*DiLon06*
	021311–1e	9595.892(6)	1.13679(8)	5.1(2)		4/4	$2\nu_2+\nu_3+(3\nu_4+\nu_5)^{0+}$	$\Sigma_u{}^+$–$\Sigma_g{}^+$	9595.892(6)	P18/R8	2.6	
		9595.9019(7)	*1.13657(2)*	*3.2(2)*	*-40(4)*	*21*	$2\nu_2+\nu_3+(3\nu_4+\nu_5)^{0+}$	$\Sigma_u{}^+$–$\Sigma_g{}^+$	*9595.9019(7)*	*P18/R16*	*1.0*	*DiLon06*
	0030000e	9609.103(2)	1.13259(3)	2.1(1)		22/26	$3\nu_3$	$\Sigma_u{}^+$–$\Sigma_g{}^+$	9609.103(2)	P17/R22	2.1	
		9609.1024(5)	*1.13275(3)*	*3.9(4)*	*66(15)*	*25*	$3\nu_3$	$\Sigma_u{}^+$–$\Sigma_g{}^+$	*9609.1024(5)*	*P35/R33*	*1.0*	*DiLon06*
	1112000e	9615.863(3)	1.13920(4)	-0.4(1)		8/9	$\nu_1+\nu_2+\nu_3+2\nu_40$	$\Sigma_u{}^+$–$\Sigma_g{}^+$	9615.863(3)	P20/R14	2.4	
		9615.8688(9)	*1.13906(2)*	*-1.4(1)*	*-19(2)*	*26*	$\nu_1+\nu_2+\nu_3+2\nu_40$	$\Sigma_u{}^+$–$\Sigma_g{}^+$	*9615.8688(9)*	*P21/R19*	*1.0*	*DiLon06*
	1112020e	9615.919(2)	1.129478(5)			17/19	$\nu_1+\nu_2+\nu_3+2\nu_4{}^2$	Δ_u–$\Sigma_g{}^+$	9615.919(2)	P24/R23	5.1	
		9615.8845(7)	*1.13004(2)*	*2.03(8)*	*22(1)*	*32*	$\nu_1+\nu_2+\nu_3+2\nu_4{}^2$	Δ_u–$\Sigma_g{}^+$	*9615.8845(7)*	*P30/R28*	*0.9*	*DiLon06*
	1020000e	9654.674(1)	1.130201(9)	1.25(1)		34/38	$\nu_1+2\nu_3$	$\Sigma_u{}^+$–$\Sigma_g{}^+$	9654.674(1)	P25/R28	2.7	
		9654.6730(3)	*1.130322(4)*	*1.64(1)*	*3.51(9)*	*50*	$\nu_1+2\nu_3$	$\Sigma_u{}^+$–$\Sigma_g{}^+$	*9654.6730(3)*	*P31/R33*	*0.9*	*DiLon06*
	2010000e	9810.942(1)	1.13050(1)	1.53(2)		40/40	$2\nu_1+\nu_3$	$\Sigma_u{}^+$–$\Sigma_g{}^+$	9810.942(1)	P26/R23	1.3	
		9810.9428(2)	*1.130526(2)*	*1.534(5)*	*-0.35(4)*	*63*	$2\nu_1+\nu_3$	$\Sigma_u{}^+$–$\Sigma_g{}^+$	*9810.9428(2)*	*P34/R33*	*0.6*	*DiLon06*

Notes. The confidence interval (1 SD) is given between parentheses, in the unit of the last quoted digit.
The spectroscopic parameters are given in cm^{-1} and for the lower levels were constrained to the values reported in Refs. [5,6,23].

[a] Normal mode labeling: $v_{i=1-5}$ are the vibrational quantum numbers, l_4 and l_5 are the vibrational angular momentum quantum numbers associated to the degenerate bending modes and $\varepsilon=e$ or f is the symmetry relative to the Wang transformation. The labeling was obtained according to the maximum value of the modulo of the expansion coefficients of the vibrational eigenfunction in the normal mode basis (for low J values)."N" identifies the newly observed bands.

[b] Square of the maximum value of the modulo of the expansion coefficients of the vibrational eigenfunction in the normal mode basis (for low J values).

[c] N_{tot} is the total number of observed transitions and n_{fit} is the number of line positions included in the fit.

[d] Plíva's notation.

[e] Band center. $\Delta G_{e/f}=G'_{e/f}-G''_{e/f}$.

[f] Observed branches with the maximum value of the total angular momentum quantum number.

[g] Root mean square deviation in 10^{-3} cm^{-1} unit. "p" marks a perturbed upper state.

[h] References to previous observations of the same band when available: *Camp05* [15], *Bég17* [4], *Herm89* [14], *JVA02* [12], *Camp03* [17], *Ding02* [18], *Weir01* [19], *DiLon06* [21].

shift on the order of 0.01 cm^{-1} for the band centers reported by Herman et al. due to an inaccurate calibration of their spectra [14].

For each upper state of the $^{12}C_2H_2$ bands, we give in Table 1 the fraction of the dominant ($v_1v_2v_3v_4v_5l_4l_5$) state of the vibrational eigenfunction, defined as the square of the maximum value of the modulo of the expansion coefficients in the normal mode basis (for low J values). Fraction values as low as 25% are noted indicating a high dilution of the vibrational eigenfunction over a number of basis states. This may be the explanation of the different vibrational assignment given in Ref. [14] to the bands near 9622.37, 9741.63 and 9909.91 cm^{-1} [14] (The latter was erroneously assigned to $\nu_1+2\nu_2+\nu_3$ in Ref. [17]).

4.2. Resonance interactions

The rovibrational analysis allowed assigning about 2050 transitions leaving 530 transitions unassigned. The unassigned lines are not believed to belong to impurities (water lines were removed and methane lines were checked to be absent). Most of them belong probably to weak $^{12}C_2H_2$ bands in particular hot bands for which the observed rotational structure is too partial for a clear identification.

The presence of a few very strong lines (intensity larger than 2×10^{-24} cm/molecule) among the unassigned dataset was puzzling. These few lines were finally identified as extra lines resulting from an intensity transfer from the very strong $3\nu_3$ band. A detailed analysis using GSCD relations allowed assigning the $R(19)$–$R(21)$ and $P(21)$–$P(22)$ extra lines accompanying the corresponding $3\nu_3$ lines which are stronger by one order of magnitude or more (The extra lines are incorporated to the $3\nu_3$ dataset provided in the Supplementary Material). In the upper panel of Fig. 3, we present the deviations relative to the positions calculated using the $3\nu_3$ band parameters for the measured positions of the $3\nu_3$ lines and for the extra lines. A clear level crossing is observed between $J_{up}=20$ and 21. Let us underline that the $3\nu_3$ line positions of interest were not measured in this work but are due Vander Auwera et al. [12] who reported their values with an accuracy of about 3×10^{-4} cm^{-1}. The shift of the $3\nu_3$ line positions from their unperturbed values ranges between -0.017 and $+0.009$ cm^{-1} which is largely above the position accuracy. Vander Auwera et al. simply excluded the perturbed lines from their fit of the spectroscopic parameters. We note that in the case of the $3\nu_3$ band, the HITRAN list judiciously reproduces the experimental position values of Ref. [12] (when available) instead of values calculated using band parameters. While in the case of an isolated band, band parameters allow for a statistical averaging of experimental uncertainties, in the present case it would have decreased the quality of the position values.

Fig. 3 (lower panel) presents the deviations from their unperturbed values of the $3\nu_3$ line positions predicted by the global effective Hamiltonian model [10,11]. As showed by the zooms presented in Fig. 4, a position shift is predicted by the global model around $J_{up}=20$ but with a significantly smaller amplitude and a slight shift along the J scale. Additional small perturbations (<0.02 cm^{-1}) are observed in Figs. 3 and 4 around $J_{up}=8$, 16, 33 and 38 and firmly confirmed by GSCD relations between the $R(J_{up}-1)$ and $P(J_{up}+1)$ positions. The occurrence of such perturbations is expected to be come more frequent at high energy as a result of the increased frequency of energy crossing with dark states. No doubt that a number of extra lines resulting from such local resonance interaction are present among the set of unassigned lines.

The energy differences between the nearby dark states predicted by the global model and the $V_3=3$ state are displayed on the lower panel of Fig. 4. The vibrational assignment of the dark states is provided in the caption of the figure. This plot gives some

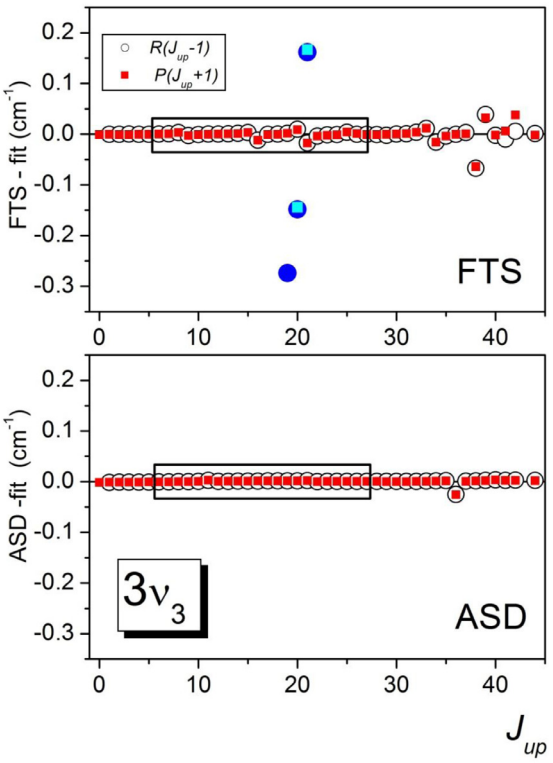

Fig. 3. Rovibrational perturbations of the $3\nu_3$ band of $^{12}C_2H_2$.
Upper panel: Deviations of measured line position values from values calculated using isolated band spectroscopic parameters *versus* the upper state J values. Circles and squares correspond to transition wavenumber of the $R(J_{up}-1)$ and $P(J_{up}+1)$ lines, respectively. Experimental position values are from Ref. [12] and this work below and above $J_{up}=28$, respectively. Blue symbols around $J_{up}=20$ show extra lines of the perturber observed through an intensity transfer.
Lower panel: Same as upper panel for the line position values predicted by the effective Hamiltonian model as provided by the Acetylene Spectroscopic Database (ASD) [11]. The rectangles indicate the enlarged zone displayed on Fig. 4. (For interpretation of the references to color in this figure legend, the reader is referred to the web version of this article.)

qualitative insight on the observed perturbations. For instance, it is interesting to note that $V_3=3$ stretching state being the most anharmonic in the region, all the nearby dark states have larger rotational constants which leads to a ($E_{dark}-E_{V_3=3}$) energy separation increasing in J. This is in full agreement with the observations: the $V_3=3$ energy levels are pushed upward and downward before and after the energy crossing, respectively (upper panel of Fig. 4).

We note in Fig. 4 that some of the energy crossings are revealed by local perturbations. Nevertheless, most of the dark states included in Fig. 4 have a very high bending excitation (e.g. $v_4+v_5\geq10$) and are not expected to interact with the 0030000 bright state. According to the Amat Nielsen scheme, the order of the interaction term of the effective Hamiltonian is the sum of the differences of the vibrational quantum numbers of the interacting levels [24]. This general rule seems to exclude a direct coupling between the 0030000 bright state and such highly bending levels. Nevertheless, let us consider the expansion coefficients of the 020634–3 dark state ($v_1v_2v_3v_4v_5l_4l_5$ notation) which presents a level crossing with the 0030000 level at $J_{up}=20$ (red stars in Fig. 4). According to the global EH, this high bending level ($v_4+v_5=9$) has a 10 % contribution from the 0024101 basis function which weakly interacts with the 0030000 basis function through a Coriolis resonance term ($C_{3/44445}$ coupling parameter - see Ref. [10] for definition).

The unambiguous identification of the other observed perturbations seems to be even more hazardous. While at lower energy, perturbers and interaction mechanisms could be unambiguously

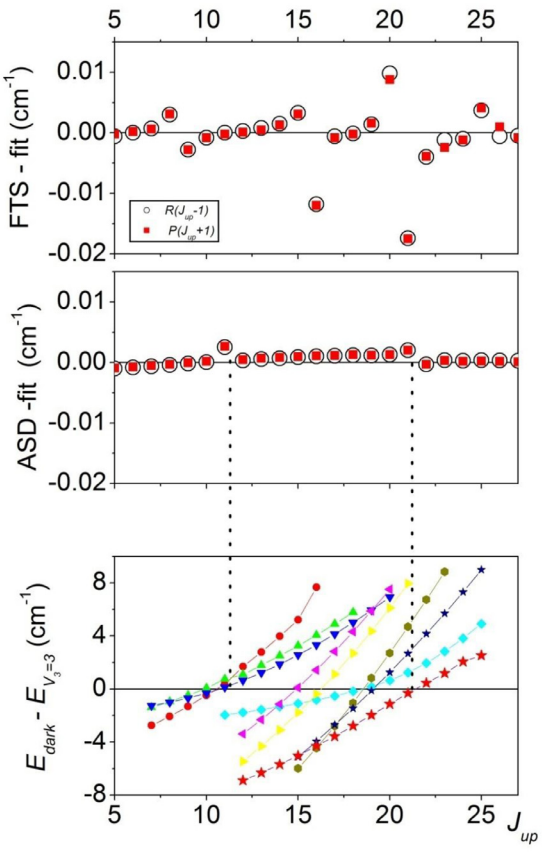

Fig. 4. Rovibrational perturbations of the $3\nu_3$ band of $^{12}C_2H_2$
Upper panels: enlargements of Fig. 3 for the J_{up} = 5–27 range.
Lower panel: Energy difference between the levels of the V_3 = 3 state and the nearby dark states as predicted by the global effective Hamiltonian [10]. Red stars correspond to the $(v_1v_2v_3v_4v_5l_4l_5)$ = (020634–3) dark state which is believed to be responsible of the perturbation of the 0030000 bright state around J_{up} = 21. The other dark states are 000(12)3(10)-3 (red circles), 100917–1 (green triangles), 110612–1a (blue triangles), 000(12)361 (pink triangles), 000(12)38–3 (yellow triangles), 110612–1b (light blue diamonds), 010935–3 (dark yellow circles), 000(12)3(12)-3 (black stars). The 110612–1a and 110612–1b states have the same dominant basis state. (For interpretation of the references to color in this figure legend, the reader is referred to the web version of this article.)

identified in a number of cases (e.g. [7]), there is much left for future work to improve the modeling of local perturbations near 1 μm.

5. Comparison to databases

5.1. Acetylene spectroscopic database (ASD)

The ASD list [11] relies on the global modelling of the $^{12}C_2H_2$ spectrum in the frame of the polyad model developed at IAO-Tomsk [10]. The most recent fitted set of 237 EH parameters was refined against about 25,000 measured line positions of about 500 bands including part of our high sensitivity studies below 7920 cm^{-1} [5,6]. Above this value, the input data of the fit was mostly limited to the few bands included in the HITRAN database. Thus the four HITRAN bands of our region were used as experimental sources of line positions. The comparison of the measured and ASD positions of the other bands provides a test of the predictive capabilities of the model. The ASD list covers the 3–10000 cm^{-1} spectral range which excludes the comparison with the $\Delta P = 16$ series of bands presently analyzed. Fig. 5 shows an overview of the deviations between the measured and ASD line positions. The deviations are less than 1 cm^{-1} and generally mostly

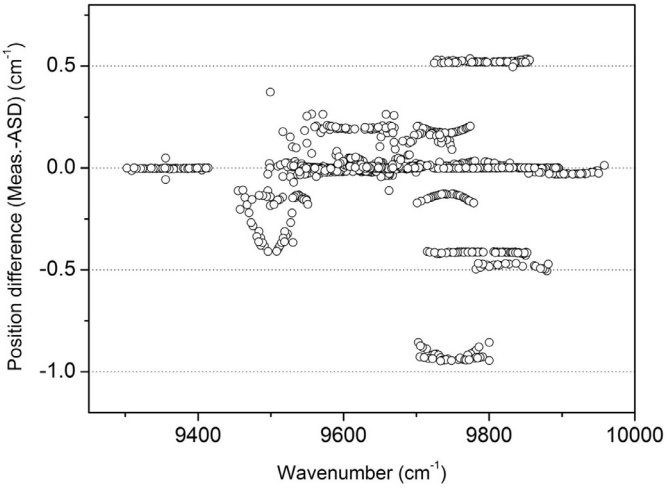

Fig. 5. Overview of the differences between the positions of the $^{12}C_2H_2$ lines assigned in the acetylene FTS spectrum between 9280 and 10740 cm^{-1} and their corresponding values predicted using the global effective Hamiltonian [10,11].

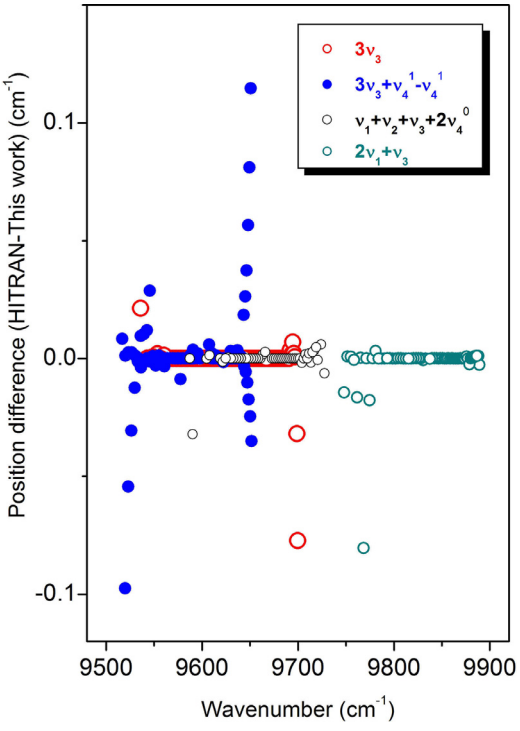

Fig. 6. Position differences between the HITRAN2016 line positions and the corresponding position values measured in this work. Different symbols are used for the four bands included in the HITRAN list.

constant for a given band indicating a small rotational dependence. In the future, the present observations will be valuable to improve the vibrational coefficients of the EH model.

5.2. HITRAN2016 database

As mentioned above, the HITRAN2016 line list provides spectroscopic information only for the four strongest bands: three Σ_u^+–Σ_g^+ bands ($3\nu_3$, $\nu_1+\nu_2+\nu_3+2\nu_4^0$, $2\nu_1+\nu_3$ at 9640, 9668 and 9835 cm^{-1}, respectively) and the $3\nu_3+\nu_4^1$-ν_4^1 Π_u–Π_g hot band at 9603 cm^{-1}. The HITRAN positions and intensities were obtained by FTS by Vander Auwera et al. [12] and Jacquemart et al. [13], respectively. In the absence of measurements for some transitions,

the HITRAN line parameters were interpolated and some high J line parameters were extrapolated (see Ref. [13]). As in our previous studies [1,2], significant deviations are observed for the extrapolated values (Fig. 6). In particular for the $3\nu_3+\nu_{41}$-ν_{41} hot band, line positions and line intensities were measured in Ref. [12,13] in the $P(20)$–$R(20)$ and $P(26)$–$R(18)$ ranges, respectively. The HITRAN list has been extended to the $P(30)$–$R(25)$ range using band parameters and Hermann Wallis coefficients for position and intensities, respectively [13]. As a result, compared to our measurements, deviations exceeding 0.1 cm^{-1} are noted for the highest J values. This is beyond the 0.01 cm^{-1} error bar (error code 3) attached to the considered HITRAN position values.

6. Conclusion

The high-resolution FTS absorption spectrum of acetylene in the 9280–10740 cm^{-1} region has been revisited. The studied region covers the $\Delta P=15$ and 16 series of bands dominated by the $3\nu_3$ and $\nu_1+2\nu_3+\nu_5{}^1$ bands near 9640 and 10364 cm^{-1}, respectively. The long path absorption spectrum under analysis combined with the high quality predictions of the global model developed at IAO-Tomsk allowed assigning a high number of new lines mostly in the $\Delta P=15$ region. Overall, 1899 $^{12}C_2H_2$ lines were assigned to thirty-three bands, twelve of them being newly reported. New or improved state parameters were derived from a fit of the measured positions values. As a result, about half of the bands were found affected by local perturbations. This is a consequence of the increased density of dark states in possible interaction with the observed bright states. While at lower energy, perturbers and interaction mechanisms could be unambiguously identified in a number of cases using the global effective Hamiltonian approach (e.g. [5,7]), in the considered region, the identification of the perturber becomes more challenging. For instance, several small position perturbations affecting the $3\nu_3$ band were evidenced and discussed in relation with the energy crossing with dark levels as predicted by the global EH. The sign of the position shifts of the $3\nu_3$ perturbed lines is observed as predicted but the quantitative description of the different resonances would require refinements of the modeling of the dark states (which are all highly bending states) and of the interaction mechanisms.

Let us mention that increased accuracy on line positions allowed by sub Doppler spectroscopy reveals that small resonance effects are the rule in the near infrared spectrum of acetylene. When line centers are measured with a very high accuracy (for instance 10^{-6} cm^{-1} or 30 kHz), small perturbations, unambiguously confirmed by GSCD, are usually evidenced in the case of energy crossings with a dark state [25,26].

The studied spectral region corresponds to the upper energy region of the bands fitted by the global EH model [10,11]. Differences up to 1 cm^{-1} are found between the EH predictions and the present measurements. The obtained set of line positions will be valuable to refine the set of EH parameters and improve the quality of the predictions at higher energy. The comparison to the line list provided by the HITRAN2016 indicates that the HITRAN list includes a number of high J position values which were inaccurately extrapolated (deviations up to 0.1 cm^{-1}).

Additional work on line intensities is planned in order construct an empirical line list for acetylene near 1 µm, suitable for spectroscopic databases. Following the approach of Ref. [1], Herman–Wallis coefficients will be derived for completing the experimental list by adding missing lines and improving poorly determined intensities. In addition, we plan to improve the $\Delta P=15$ effective dipole moment parameters and to determine for the first time the $\Delta P=16$ EDM parameters.

Acknowledgments

The supports of the CNRS (France) and RFBR (N16-55-16017) in the frame of Laboratoire International Associé SAMIA are acknowledged. O.L thanks Université Grenoble Alpes for a two-months support at LIPhy Grenoble. This work was performed in the frame of the LabexOSUG@2020 (ANR10 LABX56) and of the ANR project e_PYTHEAS (ANR-16-CE31-0005).

Supplementary materials

Supplementary material associated with this article can be found, in the online version, at doi:10.1016/j.jqsrt.2018.01.007.

References

[1] Lyulin O.M., Campargue A. An empirical spectroscopic database for acetylene in the regions of 5850–6341 cm^{-1} and 7000–9415 cm^{-1} 2017;203:461–471. 10.1016/j.jqsrt.2017.01.036
[2] Lyulin OM, Vander Auwera J, Campargue A. The Fourier transform absorption spectrum of acetylene between 7000 and 7500 cm^{-1}. J Quant Spectrosc Radiat Transf 2015;160:85–93.
[3] Lyulin OM, Vander Auwera J, Campargue A. The Fourier transform absorption spectrum of acetylene between 8280 and 8700 cm^{-1}. J Quant Spectrosc Radiat Transf 2016;177:234–40. http://dx.doi.org/10.1016/j.jqsrt.2015.11.026.
[4] Béguier S, Lyulin OM, Hu SM, Campargue A. Line intensity measurements for acetylene between 8980 and 9420 cm^{-1}. J Quant Spectrosc Radiat Transf 2017;189:417–20. doi:10.1016/j.jqsrt.2016.12.020.
[5] Lyulin OM, Campargue A, Mondelain D, Kassi S. The absorption spectrum of acetylene by CRDS between 7244 and 7918 cm^{-1}. J Quant Spectrosc Radiat Transf 2013;130:327–43.
[6] Lyulin OM, Mondelain D, Béguier S, Kassi S, Vander Auwera J, Campargue A. High sensitivity absorption spectroscopy of acetylene by CRDS between 5851 and 6341 cm^{-1}. Mol Phys 2014;112:2433–44.
[7] Kassi S, Lyulin OM, Béguier S, Campargue A. New assignments and a rare peculiarity in the high sensitivity CRDS spectrum of acetylene near 8000 cm^{-1}. J Mol Spectrosc 2016;326:106–14.
[8] Gordon IE, Rothman LS, Hill C, Kochanov RV, Tan Y, Bernath PF, et al. The HITRAN2016 molecular spectroscopic database. J Quant Spectrosc Radiat Transfer 2017;203:3–69. https://doi.org/10.1016/j.jqsrt.2017.06.038.
[9] Jacquinet-Husson N, Armante R, Crépeau N, Chédin A, Scott NA, Boutammine C, et al. The 2015 edition of the GEISA spectroscopic database. J Mol Spectrosc 2016;327:31–72. doi:10.1016/j.jms.2016.06.007.
[10] Lyulin OM, Perevalov VI. Global modelling of vibration-rotation spectra of acetylene molecule. J Quant Spectrosc Radiat Transf 2016;177:59–74.
[11] Lyulin OM, Perevalov VI. ASD-1000: high-resolution, high-temperature acetylene spectroscopic databank. J Quant Spectrosc Radiat Transf 2017;201:94–103.
[12] Vander Auwera J, Hachtouki El R, Brown LR. Absolute line wavenumbers in the near infrared: $^{12}C_2H_2$ and $^{12}C^{16}O_2$. Mol Phys 2002;100:3563–76.
[13] Jacquemart D, Lacome N, Mandin JY. Line intensities of $^{12}C_2H_2$ in the 1.3, 1.2 and 1 μm regions. J Quant Spectrosc Radiat Transfer 2009;110:733–42.
[14] Herman M, Huet TR, Vervloet M. Spectroscopy and vibrational couplings in the $3\nu_3$ region of acetylene. Mol Phys 1989;66:333–53.
[15] Campargue A, Wang L, Cermak P. Hu S-M. ICLAS-VeCSEL and FTS spectroscopies of C_2H_2 between 9000 and 9500 cm^{-1}. Chem Phys Lett 2005;403:287–92.
[16] Bertseva E, Campargue A. Spectral condensation near molecular transitions in ICLAS-VeCSEL. Optics Com 2004;232:251–61.
[17] Campargue A, Bertseva E, Ding Y. The overtone spectrum of of C_2D_2 and C_2H_2 by ICLAS–VECSEL near 1 µm. J Mol Spectrosc 2003;220:13–18.
[18] Ding Y., Herman M., Campargue A.. ICLAS of $^{12}C_2H_2$ between 10140 and 10600 cm^{-1}, J Mol Spectrosc 2002;211:1–5.
[19] Weirauch G, Campargue A, El Idrissi MI, Herman M. The absorption spectrum of $^{12}C_2H_2$ IV. The regions 7600–9200 cm^{-1} and 10600–11500 cm^{-1}. Mol Phys 2001;99:143–9.
[20] Lyulin OM, Perevalov VI. Effective dipole moment parameters of $^{12}C_2H_2$ for the100, 7.7, 1.4, 1.3, 1.2 and 1.0 μm regions. J Mol Spectrosc 2011;266:75–80.
[21] Di Lonardo G, Fusina L, Tamassia F, Fayt A, Robert S, Vander Auwera J, et al. The FT absorption spectrum of $^{13}CH^{12}CH$ (II): rotational analysis in the range 9500–10000 cm^{-1}. Mol Phys 2006;104:2617–25.
[22] Robert S. PhD thesis Université Libre de Bruxelles (2009).
[23] Di Lonardo G, Baldan A, Bramati G, Fusina L. The infrared spectrum of $^{12}C^{13}CH_2$: the bending states up to $\nu_4+\nu_5=4$. J Mol Spectrosc 2002;213:57–63.
[24] Amat G, Nielsen HH, Tarrago G. Rotation-vibration of polyatomic molecules. New York: Dekker; 1971.
[25] Twagirayezu S, Cich MJ, Sears TJ, McRaven CP, Hall GE. Frequency-comb referenced spectroscopy of ν_4- and ν_5-excited hot bands in the 1.5 µm spectrum of C_2H_2. J Mol Spectrosc 2015;316:64–71.
[26] Tao LG, Hua TP, Sun YR, Wang J, Liu AW, Hu SM. Frequency metrology of the acetylene lines near 789 nm. J Quant Spectrosc Radiat Transf 2018 Submitted for publication.